

8B.1 RECENT SEVERE WEATHER EVENTS OVER APULIA REGION OBSERVED BY NEWLY INSTALLED C-BAND POLARIMETRIC DOPPLER RADAR OF THE RIVONA PROJECT

F. Prodi, F. Congedo, F. Pasqualucci, G. Trivellone
Institute of Atmospheric Sciences and Climate – National Research Council, Bologna, Italy

1. INTRODUCCION

The Mediterranean Sea is frequently struck by high impact severe weather events causing disasters and serious threats for human safety in the surrounding regions. Numbers of violent meteorological events, such as flash-floods, devastating hailstorms as well as tropical-like cyclones have been reported in the literature over Mediterranean region [1] – [4]. In spite of being a relatively small basin, several physical mechanisms turned up to be favourable to initiate and emphasize convection: latent-heat supply, intricate orography, frequent humid south winds are just some key factors that can bring about severe Mediterranean cyclonic activities [5] – [9].

Obviously, in this scenario, the development of a suitable weather radar network has been playing an increasingly importance in supporting daily operations of forecasting centres. In fact, the detailed description of current weather conditions provided by radar echoes, combined with remote sensing data from satellite, GPS, wind profiler and lightning, are a powerful tool for implementing pervasive and efficient nowcasting systems [10, 11].

The strength of radar-based nowcasting and, in broad terms, of early-warning systems lies in real-time monitoring and accurate tracking over large areas of high-impact weather phenomena such as tornadoes, heavy rains, large hail, severe wind gusts and lightning. Therefore, extrapolation of detailed information given by doppler radars clearly plays a crucial role for the protection of people's lives and the mitigation of public and private damages due to weather hazards.

In this paper, we will focus on Apulia region, located in the Central Mediterranean Sea, in South-eastern Italy. Apulia, bordering the Adriatic Sea to the east and the Ionian Sea to the southwest (see Fig. 1), has a typical Mediterranean climate. However, although several heavy rain episodes have affected the region in the last years [12] – [14], up to now Apulia was lacking of an adequate weather radar coverage allowing for an efficient and detailed nowcasting capability over the whole regional area.

To this regard, a new C-band polarimetric doppler radar has recently been installed in Torchiariolo, around the Brindisi Airport area, within the RIVONA project [15] (more details about the project will be given in the following Section).

Despite RIVONA principally aims at improving the Brindisi airport nowcasting systems by setting up a complex real-time radars and ground-sensors network, the newly installed Torchiariolo radar is on its own a powerful tool able to detect and follow the evolution over the entire region of intense convective precipitations.



Fig. 1 Apulia region between the Adriatic Sea and the Ionian Sea.

Accordingly, by means of polarimetric doppler radar images, the present paper is aimed at describing two weather events which recently affected Apulia region. In more detail, the paper is organised in two sections: in Section 2 the RIVONA project will be briefly introduced with a focus on the technical features of Torchiariolo C-band radar; in Section 3 two relevant weather events occurred in the Mediterranean basin since radar installation are selected for the purposes of our studies. Specifically, each event will be shortly introduced by a large-scale synoptic analysis sometimes accompanied by vertical sounding in Brindisi.

Related polarimetric and Doppler radar observations will be hence presented and discussed investigating microphysical properties of clouds and precipitations. Finally, in Section 4 some conclusions will be drawn.

2. THE RIVONA PROJECT

RIVONA (“Flight risks mitigation and nowcasting at airports”) is a research project funded by Apulia region within FP7 that aims at providing a complete characterization of frequency and structure of wind-shear phenomena [16].

Specifically, RIVONA resumes the “Joint Airport Weather Studies” (JAWS), the first innovative study on microburst-type wind-shear events conducted in the early 80's near to Denver's airport (USA) [17]. However, the adoption of cutting-edge technologies not available at the time, such as dual-polarization radars and more sophisticated storm-tracking radar algorithms, represents the high-added value of the RIVONA project with respect to the JAWS experience.

Therefore, the ultimate aim of RIVONA is to develop an advanced wind-shear alert system in the Brindisi Airport area, in the southern part of Italy, able to reduce flight risks associated with wind-shear and microbursts, especially during the phases of aircraft take-off, final approach and landing [15].

* Corresponding author address: F.Prodi, Institute of Atmospheric Sciences and Climate – National Research Council, Via Gobetti 101, Bologna, Italy; e-mail: f.prodi@isac.cnr.it



Fig. 2. The RIVONA experiment site: Brindisi Airport, Apulia region.

The RIVONA framework is made up of two C-band Doppler radars, both around the airport environment, as depicted in Fig. 2. More specifically, a dual-polarization radar is located in Torchiarolo while another one, with single polarization capability, has recently been installed in Mesagne.

Furthermore, six microbarographs will be established at proper locations to detect gravity waves, while a Ka-band mobile Doppler radar and three microwave disdrometers (PLUDIX) will soon be deployed along the airport landing strip complementing the C-band radar observations of the wind-shear events [15].

2.1 Torchiarolo C-Band Dual Polarity Radar

According with the project specifications, the polarimetric C-band doppler radar at Torchiarolo site has already been operating since November 2013, whilst the installation of the second C-band radar on the Mesagne support tower has recently been completed.

Torchiarolo radar uses an Advanced Radar Corporation pedestal with a 4.2 m diameter parabolic reflector, as reported in Figure 3a. The antenna has a maximum gain of 45 dB and a 3-dB beamwidth of about 1° [18].

The microwave signal is generated by a solid state magnetron transmitter supplied by Applied System Engineering Inc (Fig. 3b). It operates at 5.625 GHz with 250 kW peak transmitted power and a maximum duty cycle of 0.001 [19].



Fig. 3. a. Parabolic reflector and b. magnetron transmitter of Torchiarolo radar.

The radar acquisition and processing chain consists of a HiQ digital receiver, also referred to as Data Acquisition (DaQ) computer, and a Moment Generator/Product Generator (MGEN/PGEN) computer equipped with the latest version of the UCAR-TITAN (Thunderstorm Identification Tracking Analysis and Nowcasting) software [20]. By controlling the transmitter, receiver, and the signal processing, the MGEN/PGEN computer represents the centre of control and data processing in the radar.

The main radar features are summarized and shown in Table I.

TABLE I
TORCHIAROLO C-BAND DUAL POLARITY RADAR FEATURES

Feature	Value
<i>Frequency</i>	5.625 GHz
<i>Beamwidth</i>	1°
<i>Antenna gain</i>	45 dB
<i>Dish diameter</i>	4.2 m
<i>Pick power</i>	250 kW
<i>Duty cycle</i>	0.001
<i>Pulse width</i>	0.4 - 2 μs
<i>PRF</i>	200 – 625 Hz
<i>Range</i>	10 – 297 Km

3. CASE STUDIES

In this Section, two major severe weather episodes, namely a flash-flood and a heavy hailstorm in Apulia region will be discussed by means of polarimetric and doppler radar observations.

3.1 Flash-Flood, 30 November – 3 December 2013

From the 30th of November to the 3rd of December 2013 Apulia was affected by broad and persistent severe weather conditions with serious threats for the safety of the population and significant damage for roads, railways and infrastructure.

Heavy rainfall caused widespread flooding and overflowing streams over the entire region; even landslides occurred in the province of Foggia, in particular in the Daunian sub-Apennine. Strong winds and huge sea-storms was reported by the Civil Protection of Apulia region as well [21].

The cyclonic circulation in the Mediterranean basin stemmed on 30 November from a deep large-scale 500 hPa trough extended from North Europe to Libyan midland, as clearly illustrated in Fig. 4a where the 500 hPa geopotential height on Saturday, 30 November at 12:00 UTC is reported. The 850 hPa temperature forecasted by the GFS numerical model for the following day at 00:00 UTC and reported in Fig. 4b shows a cold air flow moving from north-east southward down to the Sahara Desert. Consequently, a cyclonic circulation conveying warm humid air from Sicily to Greece quickly took place over the northern Libyan coast getting deeper during its northward movement toward Sicily. On the 1st of December, due to the eastward movement of the Azores High's major axis, the entire structure rapidly cut off over the Central-Western Mediterranean Sea, as reported in Fig. 4c where a 995 hPa sea-level low pressure can be seen near to southern Sicily coast.

The rainfall event firstly hit south Apulia, in particular Salento Peninsula, almost without interruption from Saturday afternoon until early morning of the following day. Fig. 5 depicts the spatial distribution of total cumulated precipitation in the aforementioned time period obtained by interpolating data recorded by weather stations of the Apulia Civil Protection: widespread and abundant rain locally up to about 60 – 70 mm was registered in the Province of Brindisi, Taranto and Lecce causing wall collapse and roads flooding [22].

While the cyclone was progressing northward during the night between Saturday 30 November and Sunday 1 December, Torchiarolo radar was operating for the first time documenting structure and evolution of the system. The sequence of reflectivity maps sampled every 20 minutes from Torchiarolo radar recordings (Fig. 6) clearly illustrates the mesoscale structure of the system embedding convective cells in a general stratified structure. In more detail, reflectivity maps show that, in this first phase of the event, Salento Peninsula dealt with persistent but mainly moderate rain without significant thunderstorm episodes reported. In fact, widespread reflectivity peaks up to 45 dBz, corresponding to a rain rate of about 25 mm/h (according to the simple Marshall-Palmer relationship [23]), were observed throughout the radar

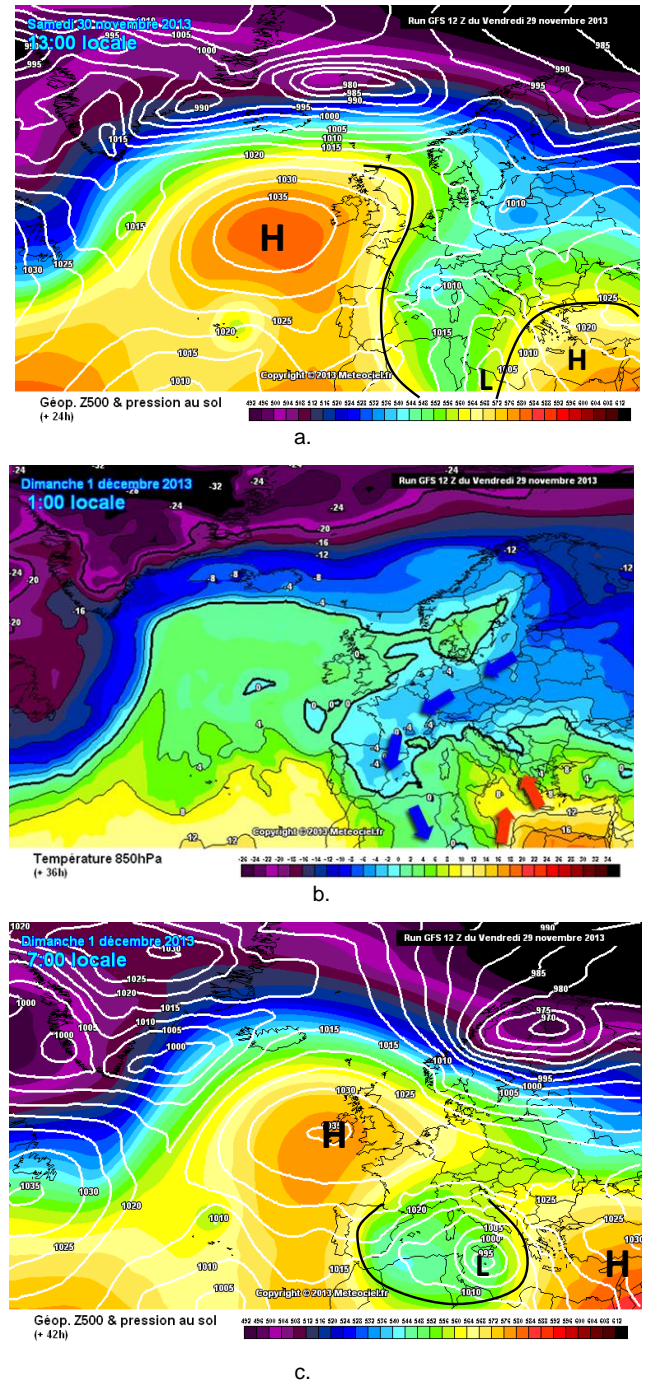


Fig. 4. Genesis and evolution of the convection system between the 30th of November and the 1st of December 2013: a. GFS 500 hPa geopotential height (in m/10, colours) and sea level pressure (in hPa, solid white lines) on 30 November 2013 at 12:00 UTC; b. 850 hPa temperature (in °C, colours) on 1 December 2013 at 00:00 UTC; c. GFS 500 hPa geopotential height and sea level pressure on 1 December 2013 at 06:00 UTC (www.meteociel.fr).

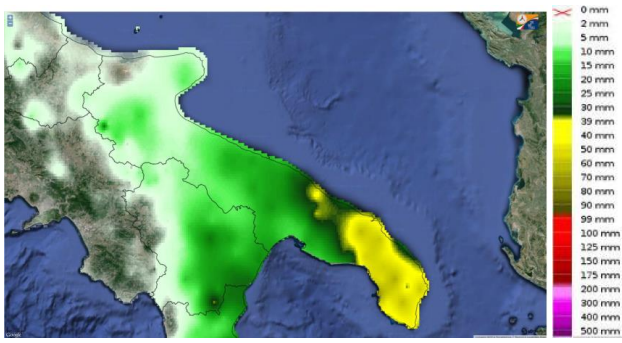


Fig. 5. Total cumulated precipitation from 12:00 UTC on 30 November to 00:00 UTC on 1 December 2013 [21].

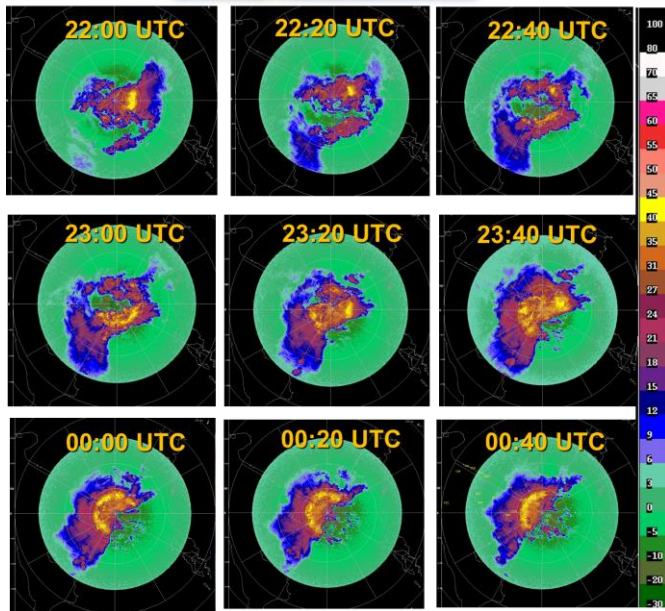


Fig. 6. Sequence of reflectivity maps (dBz) taken every 20 minutes from Torchiariolo radar recordings from 22:00 UTC on 30 November to 00:40 UTC on 1 December 2013. The radar range of observation was set to 150 Km.

range of observation (150 Km) from 22:00 UTC on 30 November to 00:40 UTC on 1 December.

In the following days, the system moved northward giving rise to severe large-scale hydrogeological phenomena in the north part of Apulia, as detailed in [21].

Init: Tue 07Oct2014 at 12Z Valid: Tue 07OCT2014 at 12Z
500 hPa Geop. Height (m) + Temp. (C) and MSL Pressure (hPa)

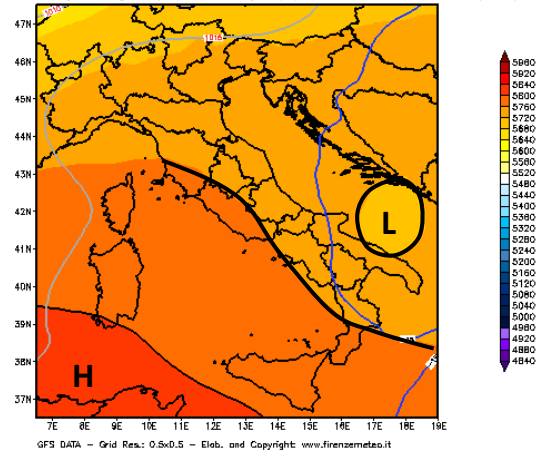


Fig. 7. GFS 500 hPa geopotential height (shaded areas) with temperature (contour lines) and sea level pressure (in hPa, grey contour lines) at 12:00 UTC on 7 October 2014 (www.firenzemeteo.it).

3.2 Heavy Hailstorm in the Itria Valley, 7 October 2014

A significant hail event was registered in the Itria Valley, in central Apulia, during the afternoon of the 7th of October 2014.

The synoptic situation forecasted by the GFS model at 12:00 UTC and reported in Fig. 7 illustrates a weak cut-off low over Southern Adriatic Sea. This cold mass at high levels (500 hPa) was contrasted with the presence of relatively warm and humid air near the surface thus favouring scattered thunderstorm activity in the warmer hours of the day. Consequently, the hail event was characterized by a moderately unstable atmosphere as can be easily detected in the thermodynamic sounding registered in Brindisi station at 12:00 UTC and reported in Fig. 8. Specifically, the analysis of some relevant convective indices, in particular CAPE, Total Totals and K Index (Table II), indicates the potential likelihood of locally severe storm episodes [24].

In addition to this, it can be observed that both the Lifting Condensation Level (LCL) and the Level of Free Convection (LFC) are located at low heights, 926.8 hPa and 861.3 hPa, respectively, thus making deep convection activity very likely to initiate and develop.

TABLE II

INSTABILITY INDICES FOR BRINDISI ON 7 OCTOBER 2014 AT 12:00 UTC

Index	Value
Lifted Index (LIFT)	-3.05 °C
Total Totals (TTOT)	51.90 °C
K Index (KINX)	25 °C
SWEAT Index (SWET)	161.2
CAPE	562 J/Kg
CIN (CINS)	-31.5 J/Kg
Showalter Index (SHOW)	0.11

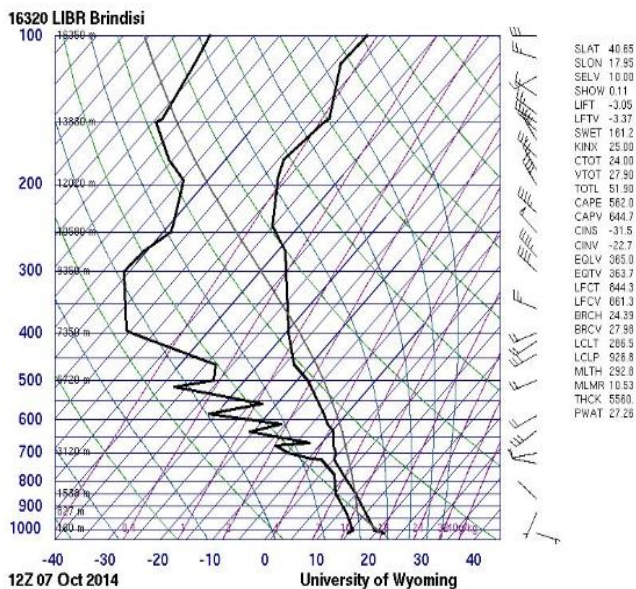


Fig. 8. Brindisi sounding plotted on a skew-T log-p diagram recorded at 12:00 UTC on 7 October, 2014. The instability indices are located in the column on the right. (University of Wyoming weather.uwyo.edu/upperair/sounding.html).

Moreover, light variable winds near the surface combined with a moderate wind shear from 700 hPa up to about 200 hPa could have played a key role in the genesis of hailstorm episodes in particular over central and southern Apulia.

Fig. 9a shows the devastation caused by an intense hailstorm which swept through the Itria Valley during the afternoon of 7 October 2014. In particular, Fasano and Ostuni were severely affected by two different storms which in few minutes made the streets completely whitewashed by a mound of ice up to 40 cm, as illustrated in Fig. 9a. Hailstones the size of walnuts are reported in Fig. 9b.

Polarimetric radar data, namely the reflectivity factor Z , the differential reflectivity Z_{DR} (defined as the logarithmic ratio of the reflectivity factors at horizontal and vertical polarizations) and the co-polar correlation coefficient ρ_{HV} between horizontal and vertical polarizations of two pulses in a given volume may be used to easily detect the presence of hail in convective storms. Additionally, by using dual-polarization data combined with vertical thermodynamic sounding it is possible to retrieve microphysical properties of hailstones.

Specifically, large hail signature is characterized by high value of Z , differential reflectivity close to zero and reduced ρ_{HV} [25].

However, it is worth underlining that, due to resonance scattering phenomena related to smaller melting hail and larger raindrops, the near-zero Z_{DR} signature typical of large hail usually is not detectable by C-band weather radar [26]. On the other hand, smaller melting hailstones retain much of their liquid melt water and hence they are generally characterized by larger values of Z_{DR} although typically smaller than those of oblate raindrops for a given Z [27]. Consequently, the best way to identify smaller melting



a.



b.

Fig. 9. Pictures taken in Fasano after the powerful hailstorm of 7 October 2014 showing: a. hail piled up so much in the streets that it resembled snow, b. hailstones the size of walnuts (www.quotidianodipuglia.it).

hailstones is to analyse value of reflectivity factor together with correlation coefficient.

To this regard, Plan Position Indicator (PPI) Torchiareolo polarimetric data in Fig. 10 taken at 0.3° elevation refers to the Itria Valley hail core moving eastward to the Adriatic Sea once it had already hit Ostuni. In more detail, reflectivity peaks above 60 dBz (Fig. 10a) combined with correlation coefficient lower than 0.8 (Fig. 10b) are a clear signature of a region with a mixture of irregular shape hydrometeors, specifically big raindrops and melting hailstones.

Moreover, positive values of Z_{DR} locally as high as 4 dB, owing to melting, smaller resonant-sized hailstones and large raindrops, as demonstrated in [28], confirm the mixed precipitation nature of the event.

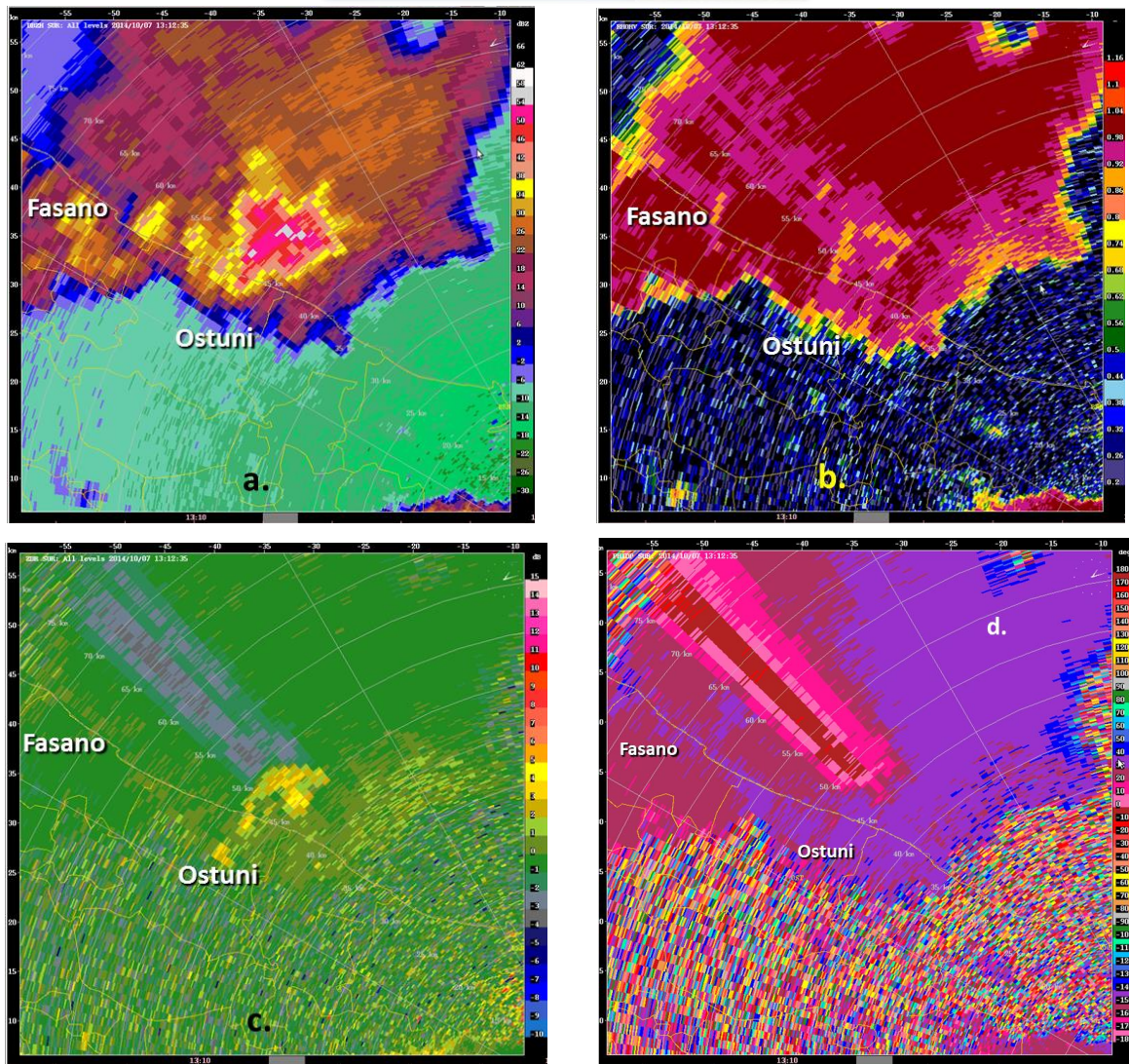


Fig. 10. Torchiarolo radar Plan Position Indicator (PPI) view taken at 0.3° elevation angle on 7 October 2014 at 13:12 UTC showing values of: a. reflectivity, b. correlation coefficient, c. differential reflectivity and d. differential phase shift of the hail core leaving Ostuni.

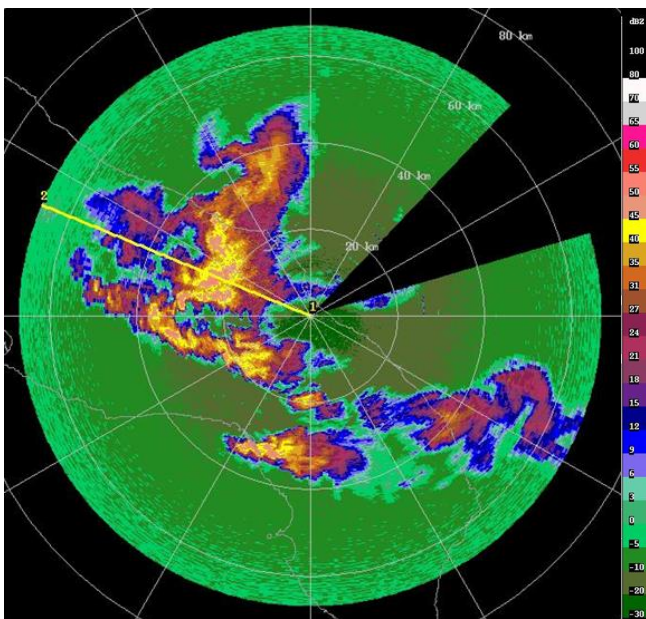


Fig. 11. PPI view taken at 1° elevation on 7 October 2014 at 14:11 UTC showing the continued development of new thunderstorm cells affecting Itria Valley as well as northern Salento. The radar observation range was set to about 60 Km.

A negative Z_{DR} shadow lengthening downrange of the hail core can be noticed in Fig 10c as well. In fact, the horizontal component of the electromagnetic wave propagating through an area with a large concentration of oblate drops and melting hailstones experiences more attenuation than the vertically polarized pulse thus introducing a significant attenuation of the differential reflectivity. Furthermore, negative Z_{DR} bias is typically accompanied by an appreciable growth of $|\Phi_{DR}|$ along the beam path, as illustrated in Fig. 10d [29].

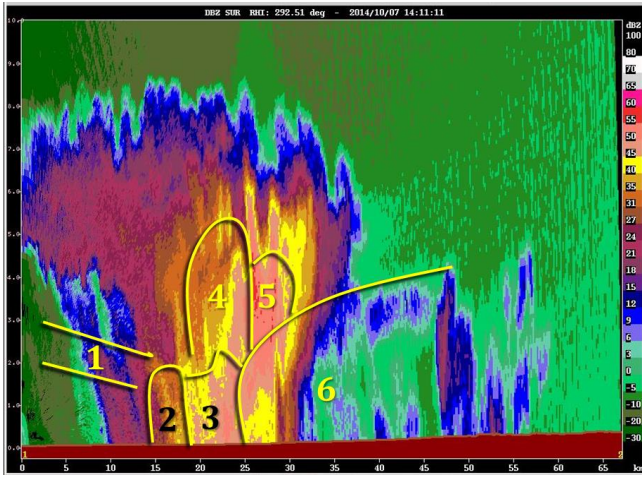
Moderate atmospheric instability conditions continued to support quite widespread convection activity until late afternoon. Torchiarolo PPI view at 1° elevation angle taken at 14.11 UTC and reported in Fig. 11 shows the continued development of locally strong cells capable of heavy rain, hail and gusty winds.

Range Height Indicator (RHI) view (see Fig. 12) showing reflectivity factor as well as polarimetric data was taken along the yellow line in Fig. 11 and corresponding to 292.52° azimuth angle.

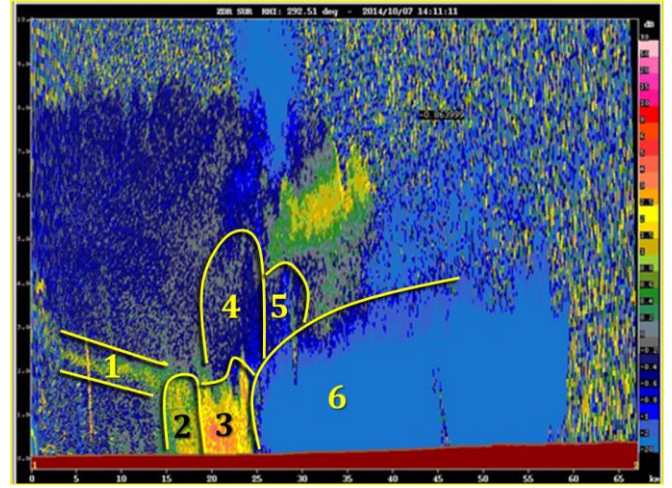
In order to characterize precipitation and discriminate hydrometeors type, size and shape, six different areas have been identified in the vertical profile of the convective cell, as illustrated in Fig. 12. A summary of dual-polarity data observed in these regions is reported in Table III.

More specifically:

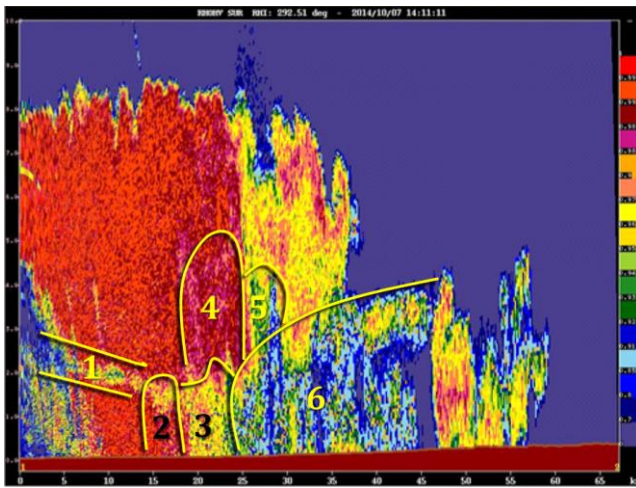
- Area 1: although no significant values of reflectivity factor can be observed, the thin horizontal strip of high differential reflectivity and low correlation coefficient is very likely to be interpreted as a melting layer zone (the freezing level is located at about 2900 m, obviously above the melting layer, as can be inferred from thermodynamic vertical profile in Fig. 8). In fact, large value of differential reflectivity, produced by melting small crystals, can be observed in a melting layer even with low value of Z_H [25].
- Area 2: by analysing polarimetric data in Table III, it can be inferred that this region, extending from the ground up to 2-Km height, is characterized by a relatively intense downpour mainly composed by medium-size raindrops. Additionally, correlation coefficient close to 1 suggests the presence of quite spherical drops.
- Area 3: this area is the most active part of the convective cell close to the ground. Increased values of both reflectivity factor and differential reflectivity together with a consistent drop of the correlation coefficient (see Table III and Fig. 12) imply heavy rainfall likely mixed with melting resonant-sized hailstones and large raindrops.
- Area 4: high reflectivity values combined with correlation coefficient close to 1 and negative values of differential reflectivity are a clear signature of dry tumbling hailstones likely mixed with graupel. In fact, the transition from near-zero to large Z_{DR} begins to occur below the freezing level which is located at about 3-Km height (Fig. 8). It is worth underlying that the transition zone corresponds in Fig. 12 to the edge between area 4 and that immediately below (area 3) which is characterized by smaller melting hailstones.
- Area 5: it is similar to area 4 except for a significant suppression of the correlation coefficient thus indicating the presence of reasonably larger hail than in area 4.



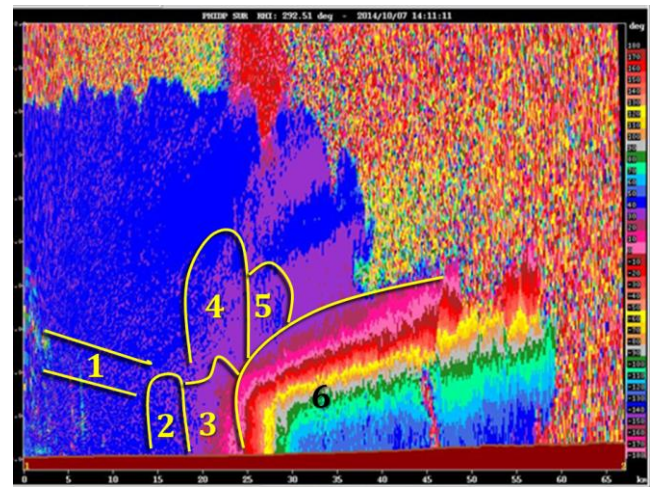
a.



b.



c.



d.

Fig. 12 Composite Range Height Indicator (RHI) views showing vertical cross-section of a. reflectivity, b. differential reflectivity, c. correlation coefficient and d. differential phase shift of the PPI image in Fig. 11 at 292.52° azimuth angle.

- **Area 6:** this area is characterized by a dramatic drop of the differential reflectivity combined with a large spread of Φ_{DR} and a substantial reduction of the copolar correlation coefficient. As previously observed in Figs. 10c and d, the horizontal channel of the radar beam crossing heavy rainfalls and melting hailstones in region 3 suffered from a significant power attenuation downrange of the core. Consequently, Z_{DR} exhibits negative values as low as -20 dB while the differential phase shift ranges from 30° to -140° and the correlation coefficient drops below 0.7, as reported in Table III. Besides the horizontal echo attenuation, large cross-beam gradients of Φ_{DR} accompanied by a noticeable decrease of ρ_{HV} may also be ascribed to a non-uniform beam filling of the region due to a gradient of precipitation types populating the radar sampling volume [30].

TABLE III
RHI POLARIMETRIC DATA OF FIGURE 12 SUBDIVIDED IN SIX DIFFERENT AREAS

Area	Z_H [dB]	Z_{DR} [dB]	ρ_{HV}	Φ_{DR} [°]
1	0 ÷ 21	-0.2 ÷ 2	0.8 ÷ 0.9	30 ÷ 40
2	21 ÷ 40	0.2 ÷ 2	0.98 ÷ 1	30 ÷ 40
3	40 ÷ 50	0.2 ÷ 5	0.85 ÷ 0.98	0 ÷ 40
4	31 ÷ 45	-1 ÷ 0	0.98 ÷ 1	30 ÷ 40
5	40 ÷ 55	-2 ÷ 0.2	0.8 ÷ 0.97	30 ÷ 40
6	0 ÷ 45	<-20	-	-140 ÷ 30

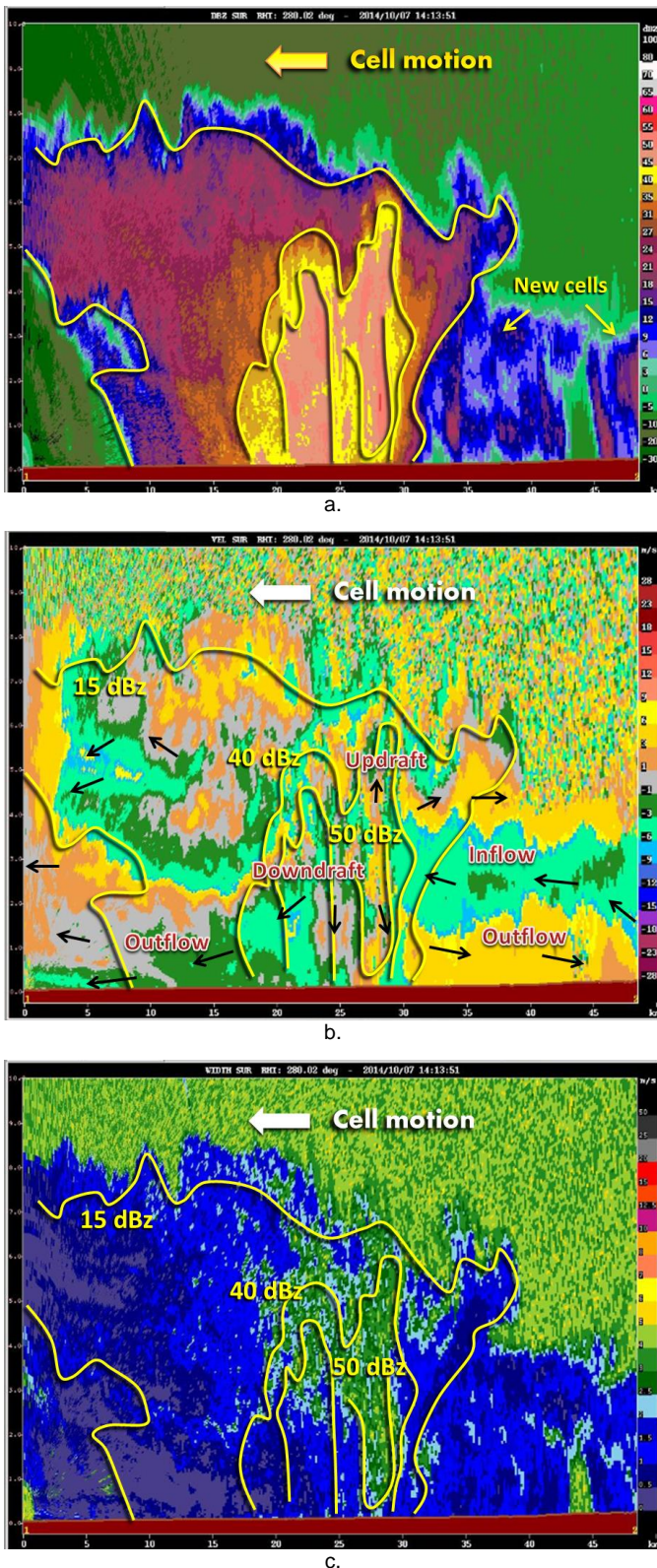


Fig. 13. RHI views taken on 7 October 2014 at 14:13 UTC showing: a. reflectivity factor, b. doppler (radial) velocity and c. spectrum width in the direction of 292.52°. Superimposed yellow lines, labelled in dBz, indicate boundaries and high reflectivity cores of the convective cell.

In Fig. 13a a vertical cross-section showing reflectivity factor, doppler velocity and spectrum width of the same convective cell of Fig. 12 is reported: the scan was taken about two minutes later at 14.13 UTC with a reduced observation range set to about 50 Km. Superimposed solid yellow lines indicate the boundary echo and high reflectivity cores of the cell.

The analysis of Doppler velocity in Fig 13b, combined with information from satellite movie, shows that the storm cell was moving south-eastward in the radar's direction following the mean wind circulation from north-west to south-east. In fact, due to the progressive movement toward south-east of the cut-off low in Fig. 7, the wind gradually started to come from the northern quadrant almost at all levels.

Grey and brown zero doppler velocity areas inside the high reflectivity core of the storm (Fig. 13b), combined with information from satellite movie, shows that the storm cell was moving south-eastward in the radar's direction following the mean wind circulation from north-west to south-east. In fact, due to the progressive movement toward south-east of the cut-off low in Fig. 7, the wind gradually started to come from the northern quadrant almost at all levels. Grey and brown zero doppler velocity areas inside the high reflectivity core of the storm (Fig. 13b) reveals the presence of the downdraft and the updraft that are, respectively, the upward-moving and downward-moving air currents flowing into the cell. Reached the ground, the downdraft radially spreads in all directions from the centre generating cold, dry air fluxes flowing radially outwards from the cell core (outflows). In particular, two outflows can be detected in Fig.13b: one, characterized by negative radial doppler velocity (green areas) was blowing toward the radar, whereas the other one was blowing away from the radar (yellow areas with positive doppler velocity) beneath a warmer and moist air current coming into the cell (inflow). Consequently, the outflow boundary forced the less dense warm air of the inflow to lift thus triggering new convection, as illustrated by the rainbands on the windward side of the storm cell in Fig. 13a.

Finally, Fig. 13c shows that the high reflectivity core of the cell exhibits greater variance of the doppler velocity than the surrounding areas: in fact, moderate values of spectrum width, locally as high as 5 m/s, are a clear signature a moderate turbulence of the air, especially at the upper levels of the core [31].

4. CONCLUSIONS

In this work a C-band dual-polarity doppler radar recently installed in Torchiarolo, Southern Apulia, Italy, has been presented and discussed. The radar was set up in November 2013 within the RIVONA Project which aims at mitigating flight risks associated with microbursts and wind shear phenomena around the Brindisi Airport area.

The analysis of polarimetric data together with doppler velocity pattern of two recent severe weather events clearly demonstrates the huge potentiality of Torchiarolo radar for monitoring high-impact weather conditions over large regional areas.

5. REFERENCES

- [1] Billing H., Haupt, I. and Tonn, W., 1983: Evolution of a hurricane-like cyclone in the Mediterranean Sea, *Beitr. Phys. Atmos.* **56**, 508–510.
- [2] Claud, C., Alhammoud, B., Funatsu, B.M., Chaboureaud, J.-P., 2010: Mediterranean hurricanes: large-scale environment and precipitating areas from satellite microwave observations, *Nat. Hazards Earth Syst. Sci.*, **10**, 2199–2213.
- [3] Laviola S., A. Moscatello, M. M. Miglietta, E. Cattani, V. Levizzani, 2011: Satellite and numerical model investigation of

- two heavy rain events over the central Mediterranean," *Journal of Hydrometeorology*, **12**, 634-649.
- [4] Funatsu B. M., C. Claud, and J.-P. Chaboureaud, 2007: Two case studies of severe storms in the Mediterranean using AMSU, *Adv. Geosci.*, **12**, 19-26.
- [5] Porcù, F., Caracciolo, C., and Prodi, F., 2003: Cloud systems leading to flood events in Europe: an overview and classification, *Met. Appl.* **10**, 217-228.
- [6] Porcù F. and A. Carrassi, Toward an estimation of the relationship between cyclonic structures and damages at the ground in Europe, 2009: *Nat. Hazards Earth Syst. Sci.*, **9**, 823-829.
- [7] Porcù, F., Carrassi, A., Medaglia, C. M., Prodi, F., and Mugnai, A., 2007: A study on cut-off low vertical structure and precipitation in the Mediterranean region, *Meteorol. Atmos. Phys.*, **96**, 121-140.
- [8] Buzzi, A., Richard, E., and Romero, R., 2005: Summary report on MEDEX studies and scientific results on Mediterranean cyclones causing high impact weather, Report on scientific results.
- [9] Levizzani V., S. Laviola, A. Malvaldi, M. M. Miglietta, and E. Cattani, 2012: Severe storms over the Mediterranean Sea: A satellite and model analysis, 6th International Precipitation Working Group, 15-20 October, Brazil.
- [10] Browning, K. A., 1982: Nowcasting. London: Academic Press.
- [11] Conway, B. J., 1998: An overview of nowcasting techniques, SAF Training Workshop – Nowcasting and Very Short Range Forecasting, EUMETSAT.
- [12] Miglietta M. M. and A. Regano, 2008: An observational and numerical study of a flash-flood event over south-eastern Italy, *Nat. Hazards Earth Syst. Sci.*, **8**, 1417-1430.
- [13] Miglietta M. M., A. Moscatello, D. Conte, G. Mannarini, G. Lacorata, R. Rotunno, 2010: Numerical analysis of a Mediterranean 'hurricane' over south-eastern Italy: Sensitivity experiments to sea surface temperature, *Atmospheric Research*, **101**, 412-426.
- [14] Mastrangelo D., K. Horvath, A. Riccio, M.M. Miglietta., 2011: Mechanisms for convection development in a long-lasting heavy precipitation event over southeastern Italy, *Atmospheric Research*, **100**, 4, 586-602.
- [15] Prodi F., G.P. Marra, F. Pasqualucci, A.C. Marra, and G. Trivellone, 2013: Meteorological risks mitigation and nowcasting at airports: the RIVONA Project," 36th Conference on Radar Meteorology, 16-20 September 2013, Breckenridge, CO.
- [16] Wilson, J.W., R.D. Roberts, C.J. Kessinger, and J. McCarthy, 1984: Microburst wind structure and evaluation of doppler radar for airport wind shear detection, *Journal of Climate and Applied Meteorology*, **23**, 898-915.
- [17] McCarthy J., J. W. Wilson, and T. T. Fujita, 1982: The joint airport weather studies project," *Bull. Amer. Meteor. Soc.*, **63**, 15-15.
- [18] Advanced Radar Corporation (ARC): www.advancedradarcorp.com.
- [19] Applied Systems Engineering, Inc. (ASE): www.applsys.com.
- [20] Thunderstorm Identification Tracking Analysis and Nowcasting (TITAN): www.ral.ucar.edu/projects/titan/home/.
- [21] Amoroso G., Evento meteo-idropluviometrico del 30 Novembre – 3 Dicembre 2013, Regione Puglia, Area Politiche per la riqualificazione, la tutela e la sicurezza ambientale e per l'attuazione delle opere pubbliche, Servizio Protezione Civile, Centro Funzionale Decentrato.
- [22] Idrografico - Protezione Civile - Regione Puglia [Available online at: www.protezionecivile.puglia.it/public/plugins/wrap/wrap.php?1].
- [23] Marshall J. S., and W. M. K. Palmer, 1948: The distribution of raindrops with size," *J. Atmos. Sci.*, **5**, 165-166.
- [24] Haklander A. J., and A. Van Delden, 2003: Thunderstorm predictors and their forecast skill for the Netherlands, *Atmos. Res.*, **67-68**, 273-299.
- [25] Kumjian M. R., 2013: Principles and applications of dual-polarization weather radar. Part I: Description of the polarimetric radar variables." *J. Operational Meteor.*, **1** (19), 226-242.
- [26] M. E. Anderson, L. D. Carey, W. A. Petersen, and K. R. Knupp, 2011: C-band dual-polarimetric radar signatures of hail, *Electronic J. Operational Meteor.*, **12** (2), 1-30.
- [27] Anderson M. E., L. D. Carey, W. A. Petersen, And K. R. Knupp, 2011: C-band dual-polarimetric radar signatures of hail, *Electronic Journal of Operational Meteorology*.
- [28] Tabary, P., C. Berthet, P. Dupuy, J. Figueras, B. Fradon, J. F. Georgis, R. Hogan, F. Kabeche, and J. P. Wasselin, 2010: Hail detection and quantification with C-band polarimetric radars: Results from a two-year objective comparison against hailpads in the south of France, 6th ERAD, Sibiu, Romania, 6-10, September 2010.
- [29] Bringi V. N., V. Chandrasekar, N. Balakrishnan, D. S. Zrnić, 1990: An examination of propagation effects in rainfall on radar measurements at microwave frequencies," *J. Atmos. Oceanic Technol.*, **7**, 829-840.
- [30] Kumjian M. R., 2013: Principles and applications of dual-polarization weather radar. Part III: Artifacts," *J. Operational Meteor.*, **1** (21), 265-274.
- [31] Rhinehart R.E., 2010: Radar for Meteorologist 5th ed., *Rhinehart Publications*.